Acta Materialia 135 (2017) 61–67

Contents lists available at ScienceDirect

Acta Materialia

journal homepage: www.elsevier.com/locate/actamat

Full length article

# Reaction of amorphous/crystalline SiOC/Fe interfaces by thermal annealing

Qing Su [a, *], Mikhail Zhernenkov [b], Hepeng Ding [c], Lloyd Price [d], Daniel Haskel [e], Erik Benjamin Watkins [f], Jaroslaw Majewski [g, h], Lin Shao [d], Michael J. Demkowicz [c], Michael Nastasi [a, i, j]

[a] Nebraska Center for Energy Sciences Research, University of Nebraska-Lincoln, Lincoln, NE 68583-0857, USA
[b] National Synchrotron Light Source II, Brookhaven National Laboratory, Upton, NY 11973, USA
[c] Materials Science and Engineering, Texas A&M University, College Station, TX 77843, USA
[d] Department of Nuclear Engineering, Texas A&M University, College Station, TX 77843-3128, USA
[e] Advanced Photon Source, Argonne National Laboratory, Argonne, IL 60439, USA
[f] Materials Synthesis and Integrated Devices, Los Alamos National Laboratory, Los Alamos, NM, USA
[g] MPA-CINT/Los Alamos Neutron Scattering Center, Los Alamos National Laboratory, Los Alamos, NM 87545, USA
[h] Department of Chemical Engineering, University of California at Davis, Davis, CA 95616, USA
[i] Department of Mechanical and Materials Engineering, University of Nebraska-Lincoln, Lincoln, NE 68583-0857, USA
[j] Nebraska Center for Materials and Nanoscience, University of Nebraska-Lincoln, Lincoln, NE 68588-0298, USA

ARTICLE INFO

*Article history:*
Received 21 February 2017
Received in revised form
3 May 2017
Accepted 8 June 2017
Available online 12 June 2017

*Keywords:*
Thermal stability
Amorphous silicon oxycarbide
Nanocrystalline Fe
Amorphous/crystalline interface

ABSTRACT

The development of revolutionary new alloys and composites is crucial to meeting materials requirements for next generation nuclear reactors. The newly developed amorphous silicon oxycarbide (SiOC) and crystalline Fe composite system has shown radiation tolerance over a wide range of temperatures. To advance understanding of this new composite, we investigate the structure and thermal stability of the interface between amorphous SiOC and crystalline Fe by combining various experimental techniques and simulation methods. We show that the SiOC/Fe interface is thermally stable up to at least 400 °C. When the annealing temperature reaches 600 °C, an intermixed region forms at this interface. This region appears to be a crystalline phase that forms an incoherent interface with the Fe layer. Density functional theory (DFT) Molecular dynamics (MD) is performed on the homogeneous SiFeOC phase to study the early stages of formation of the intermixed layer. Both experimental and simulation results suggest this phase has the fayalite crystal structure. The physical processes involved in the formation of the intermixed region are discussed.



## 1. Introduction

Deployment of the next generation of fission reactors depends on the development of new, radiation tolerant materials [1,2]. To mitigate radiation damage and suppress radiation induced dimensional and property changes, different kinds of interfaces and grain boundaries have been introduced to act as defect sinks in crystalline solids. For example, interfaces between nanoscale oxides particles and the metal matrix in oxide dispersion strengthened (ODS) steels have shown enhanced swelling and creep resistance [3,4]. Grain boundaries in nanocrystalline metals have proven to assist defect annihilation and enhance radiation resistance [5,6]. Several incoherent interfaces in nanoscale metallic laminates, including Cu/Nb [7,8], Cu/V [9], and Fe/W [10], have been demonstrated to be strong defect sinks to mitigate radiation-induced damage. In all of these attempts to improve radiation resistance in crystalline and nanocrystalline materials, interfaces were used to reduce the concentration of point defects—vacancies and interstitials—generated during irradiation.

An alternate approach to point defect removal is to develop thermally stable materials that inherently do not exhibit point defects. Amorphous materials, by definition, do not generate vacancies and interstitials during irradiation, but rather fluctuations in free volume that can easily recover *via* relaxation [11]. Silicon

* Corresponding author.
*E-mail addresses:* qsu3@unl.edu (Q. Su), zherne@bnl.gov (M. Zhernenkov).

http://dx.doi.org/10.1016/j.actamat.2017.06.020
1359-6454/

oxycarbide (SiOC) is an amorphous material displaying radiation tolerance and a very high crystallization temperature. Previous results have demonstrated that SiOC possesses good thermal and irradiation stability over a wide range of compositions, irradiation doses, and irradiation temperatures [12–14]. The material showed no evidence of crystallization up to a temperature of 1200 °C for an annealing time of 2.0 h. In addition, SiOC films remain amorphous after both light ion (He) and heavy ion (Kr) irradiation within a wide envelope of irradiation.

For potential service in extreme irradiation environments, amorphous SiOC may be combined with a crystalline metal component, such as a conventional steel, for better heat conductivity and improved mechanical properties [1,15]. Similar to interfaces in metallic nanolaminates [7,16], the amorphous/crystalline interfaces in SiOC/metal composites are expected to be strong sinks for defects, thus reducing radiation damage in the crystalline component. Previous studies have shown that SiOC/$\alpha$-Fe composites are stable after irradiation to over 30 displacements per atom (dpa) at room temperature [15,17]. In addition to radiation stability, thermal stability of the composite is another key factor to consider for its potential application in reactors with operating temperatures over 500 °C [18–23]. The understanding of the reaction at SiOC/Fe amorphous/crystalline interfaces is crucial to the development of radiation tolerant materials for service in extreme harsh environments. Therefore, in this study we present an experimental investigation of the local structure of a SiOC/Fe amorphous ceramic/metal heterophase interface after different thermal annealing conditions using a combination of x-ray and neutron reflectometry (XRR, NR), Rutherford backscatter spectroscopy (RBS), and transmission electron microscopy (TEM). These experimental results are combined with first-principles calculations to provide insight into the structural evolution of the SiOC/Fe interface after different thermal treatments.

## 2. Experimental

SiOC/Fe bi-layer films were fabricated by magnetron sputtering of SiOC and Fe onto a surface oxidized Si substrates with top $SiO_2$ layer thickness of 300 nm. The nominal thickness of the SiOC and Fe layers is 120 and 80 nm, respectively. Direct current (DC) magnetron sputtering was used to prepare nanocrystalline Fe layers first, then an amorphous SiOC layer was deposited by radio frequency (RF) co-sputtering from $SiO_2$ and SiC targets. Both layers were deposited at room temperature. A base pressure of $6.5 \times 10^{-5}$ Pa or lower was obtained prior to depositions and the Ar partial pressure during deposition was ~0.65 Pa.

To examine the thermal annealing effect, the SiOC/Fe bi-layer films were annealed in a vacuum furnace at 200, 400 and 600 °C for 1 h. Prior to annealing, the vacuum furnace pressure was below $5 \times 10^{-7}$ Pa. The cross-sectional microstructures of SiOC/Fe multilayers before and after annealing were characterized by TEM using a FEI Tecnai G2 F20 TEM. The typical TEM operating voltage was 200 kV. Cross-sectional specimens were first prepared by conventional dimpling and grinding followed by ion-milling. Low energy (3.5 keV) and low angle (5°) were selected to reduce ion milling damage.

XRR measurements were done at the 4-ID-D beamline of the Advanced Photon Source (APS) at Argonne National Laboratory with an incident photon energy of 14 keV (0.08856 nm wavelength). Unlike TEM, XRR averages over the footprint of the x-ray beam on the sample, which in this experiment was about 10 mm (L) x 200 μm (W), while providing high spatial resolution in the direction perpendicular to the interface. In XRR, a tightly collimated beam impinges on a sample at a shallow angle (typically, up to a few degrees). Specularly reflected intensity is then measured as a function of the incident angle. For the modeling of XRR curves we utilized the dynamic Parratt formalism [24] combined with a genetic fitting algorithm using the MOTOFIT software [25]. As a result of the fitting procedure, the scattering length density (SLD) profile of the sample in the direction perpendicular to the interface is obtained. SLD, which is equal to the electron density multiplied by classical electron radius, may be used to determine the average thickness of each layer and the interfacial roughness with Angstrom-level resolution, as well as chemical composition of the layers and their density. Complementary to XRR, we also performed NR measurements using the time-of-flight (ToF) reflectometer (Asterix) at the Lujan Neutron Scattering Center at Los Alamos National Laboratory. The measurement principle in NR is very similar to XRR, except that in a ToF instrument such as Asterix, specularly reflected intensity is measured as a function of the incident wavelength of neutrons at a fixed incident angle.

RBS measurements were performed at the Texas A&M University ion beam laboratory using a 1.7 MV Ionex Tandem accelerator. A beam of 2 MeV He ions was focused and collimated down to a spot size of 0.7 mm on the sample surface. The energy of backscattered He ions was measured using a semi-conductor detector at an angle of 160° from the beam. For analysis, the sample was tilted 45° in relation to the beam, towards the detector. This was done to enhance the depth resolution of the RBS probe. Energy resolution for this setup is measured at 16 keV. RUMP V4.01 was used to model the raw spectra [26,27]. This analysis provided information on the inter-diffusion between layers, the composition throughout the near-surface region, and the density-thickness product of each layer.

Our *ab initio* thermal annealing calculations were performed in cubic supercells with lattice constant of 27 Å × 27 Å × 27 Å using VASP [28], a plane wave based first-principles DFT code. The model contains 1472 atoms with a uniform composition $Si_{256}Fe_{256}O_{576}C_{192}H_{192}$, constructed to represent the mixing of 50% $Fe_2SiO_4$ and 50% SiOC:H. Starting from amorphous $SiO_2$, we reach the desired composition by substituting Fe atoms for individual SiO complexes and CH complexes for individual O atoms. We employed the Perdew-Burke-Ernzerhof (PBE) [29] exchange-correlation functional within projector-augmented-wave approach [30], a gamma-point only K point mesh, a 400 eV plane wave kinetic energy cutoff, and an energy convergence threshold of $10^{-4}$ eV for the electronic self-consistent loop. An energy convergence criterion of $10^{-3}$ eV was used for ionic relaxations within the conjugate gradient minimization scheme. A 1 fs time step and NVT ensemble with Langevin thermostat [31] were used for thermal annealing of the models. The annealing processes were performed in 100 K increments from 0 K to 900 K with a 0.5 ps equilibration after each temperature increment.

## 3. Results

### 3.1. TEM characterization of SiOC/Fe interfaces

A cross-sectional TEM micrograph of the as-deposited SiOC/Fe bilayer is shown in Fig. 1a. The Fe layer shows a columnar structure with an average grain size of 14 ± 1.2 nm while the SiOC layer exhibits uniform contrast. The columnar structure of the as-deposited Fe layer defines the intrinsic roughness at the SiOC/Fe interface. The corresponding selected area diffraction (SAD) pattern (inset of Fig. 1a) exhibits a diffuse halo around the central beam and diffraction spots along several distinct rings. The SAD confirms the body-centered cubic (BCC) structure of the Fe layer and the amorphous nature of the SiOC layer. The structural evolution of the SiOC/Fe bilayer sample after 1 h annealing at 200, 400 and 600 °C is presented in Fig. 1b, c and 1d, respectively. After 200 °C annealing

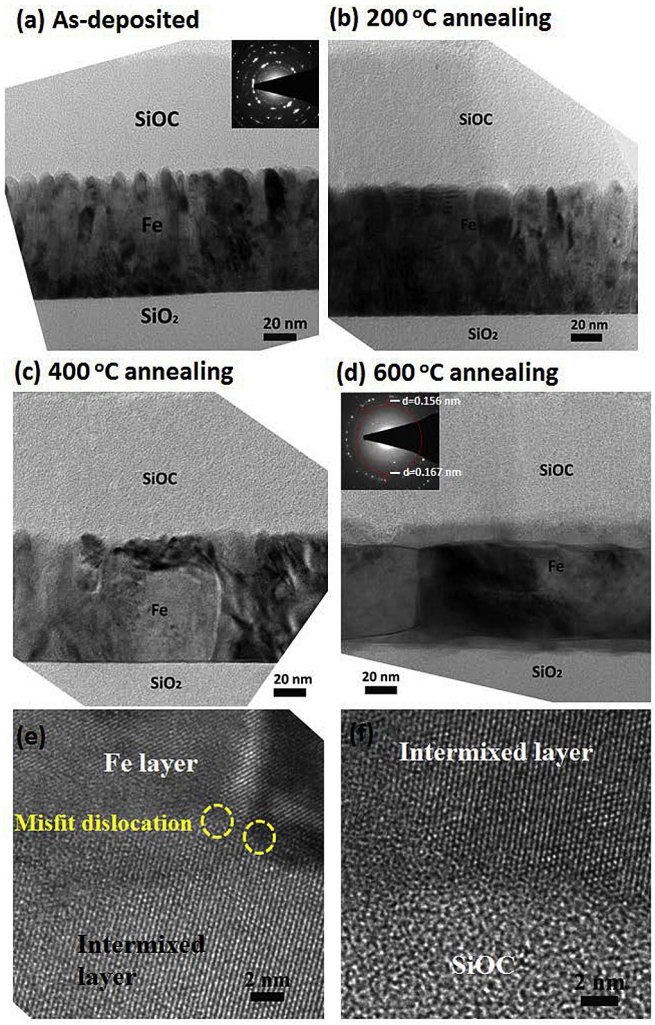


**Fig. 1.** Typical cross-sectional TEM image of Fe/SiOC bilayer specimen (a) before and after (b) 200 °C, (c) 400 °C and (d) 600 °C annealing for 1 h. High resolution TEM images of the (e) Fe/intermixed layer interface and (f) SiOC/intermixed layer interface.

for 1 h, the grain size within the Fe layer has grown from 14 ± 1.2 nm to 21 ± 2.3 nm with a simultaneous smoothening of short-range inhomogeneities at the SiOC/Fe interface, indicating that the as-deposited, zigzag SiOC/Fe interface is a thermodynamic non-equilibrium state. As the annealing temperature increases, the average Fe grain size grows, exceeding 100 nm at 600 °C.

At 600 °C, the SiOC/Fe interface thickens significantly and exhibits the formation of a well-defined intermixed layer. The corresponding SAD pattern (inset of Fig. 1d) demonstrates an extra diffraction ring and several diffraction spots, indicating the formation of an additional phase. The d-spacing for these diffraction spots and the extra diffraction ring are calculated as 0.156 ± 0.002 nm and 0.167 ± 0.001, respectively. The high resolution TEM image at Fe/intermixed layer and intermixed layer/SiOC interfaces are shown at Fig. 1e and f, respectively. These images show that the intermixed layer is crystalline and forms an incoherent interface with both Fe and SiOC layers. To interpret these findings, we propose that the intermixed region forms a layer of crystalline fayalite ($Fe_2SiO_4$). As will be shown below, our remaining experimental and modeling results are also consistent with the presence of fayalite at the SiOC/Fe interface after annealing at 600 °C.

### 3.2. STEM characterization of intermixed region at SiOC/Fe interfaces

To examine the chemical composition of the intermixed layer between Fe and SiOC, scanning transmission electron microscopy (STEM) and X-ray spectroscopy (EDS) line scans were performed. Fig. 2a shows a STEM image of the SiOC/Fe bilayer sample after 1 h annealing at 600 °C. The contrast of the interfacial region is intermediate between that of the Fe and SiOC layers. Because contrast in STEM mode is roughly proportional to the atomic number squared ($Z^2$, also called Z-contrast imaging), this result confirms intermixing between the two layers at the interface. EDS line scans across the whole specimen as well as close to the Fe/$SiO_2$ (substrate) and SiOC/Fe interfaces are shown in Fig. 2b, c, and 2d, respectively. This measurement shows that the thickness of the intermixed layer at the SiOC/Fe interface is about 14 nm. The concentration of Si in this intermixed layer is almost constant, while the concentration of Fe varies slightly, decreasing as a function of distance away from the Fe layer. The Fe-to-Si ratio at the interface is roughly 2:1, consistent with that of fayalite ($Fe_2SiO_4$). The EDS scan in Fig. 2c shows that there is also a 5 nm-thick intermixed region between the Fe layer and $SiO_2$ substrate after 600 °C annealing.

## 4. Discussion

### 4.1. XRR

The TEM, STEM, and EDS results presented above were further substantiated with XRR. The experimental curves for both as-deposited and annealed samples and the corresponding scattering length density profiles (SLDs) obtained from the fitting procedure are shown in Figs. 3 and 4, respectively. The model parameters are summarized in Table 1. Compared with the as-deposited state, there is no significant change in the SiOC and Fe layers after annealing at 200 °C and 400 °C, which is in good agreement with the TEM results. Upon annealing at 200 °C, the thickness of the SiOC layer decreases by about 7% and its physical density increases by about 4%. Together with the 15% thickness increase of the interfacial region between SiOC and Fe (denoted in the table as "SiOC + Fe"), this result suggests some limited intermixing of the two layers at the interface at this temperature. The Fe/

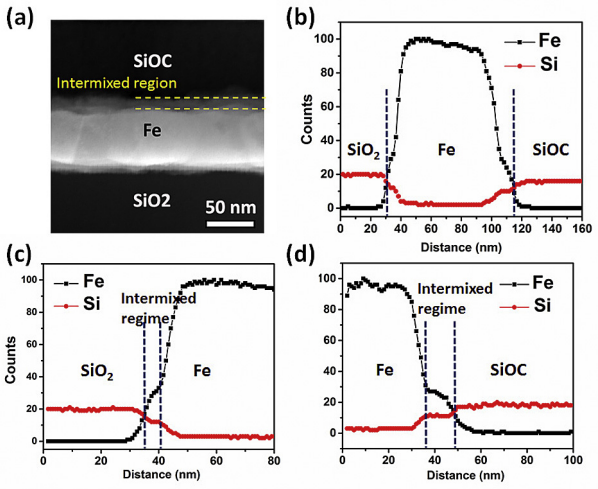


**Fig. 2.** (a) High resolution STEM image and line scan of the Fe/SiOC bilayer specimen after 600 °C annealing for 1 h. The typical EDS line scan yield of the (b) whole specimen, (c) regime close to Fe/$SiO_2$ interface, and (d) regime close to Fe/SiOC interface.

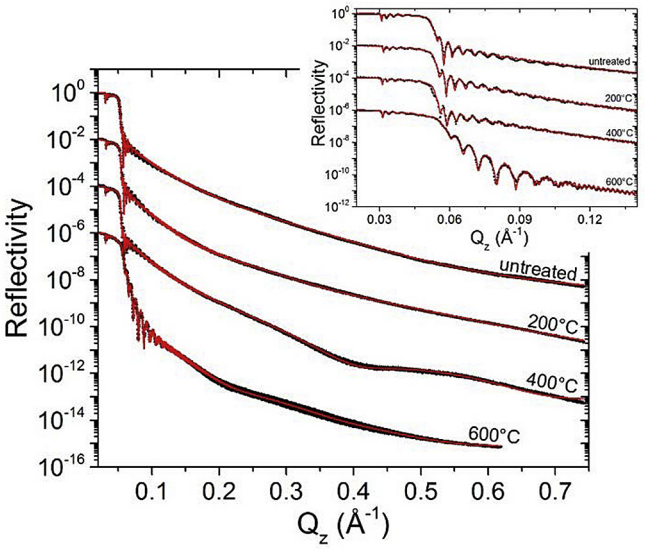


**Fig. 3.** XRR curves (black dots) and the corresponding fitting curves (red solid lines) for the untreated sample and samples annealed at 200 °C, 400 °C, and 600 °C. The insert shows the close-ups of curves up to $Q_z = 0.14$ Å$^{-1}$ to highlight the fit quality and the reflectivity curve modulations due to the different layers (SiOC, Fe, and $SiO_2$) within this region of interest. XRR curves are offset for clarity. (For interpretation of the references to colour in this figure legend, the reader is referred to the web version of this article.)

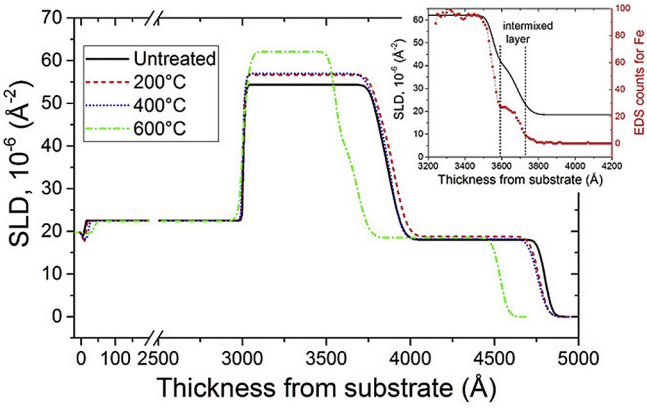


**Fig. 4.** X-ray SLD profiles obtained from the X-ray reflectivity fits. Zero in the horizontal axis corresponds to Si substrate. To clearly show the structural evolution of the SiOC/Fe bilayer, the break introduced into the horizontal scale between 200 Å and 2800 Å was located entirely within the $SiO_2$ layer. The inset compares the EDS Fe line scan (red dots with the scale to the right) with the XRR SLD at 600 °C (solid black line with the scale to the left). The 132 Å-thick intermixed layer is shown by dashed vertical lines. (For interpretation of the references to colour in this figure legend, the reader is referred to the web version of this article.)

$SiO_2$ interface remains sharp up to 400 °C, exhibiting sub-nm thickness.

According to TEM, the morphology of the Fe layer changes noticeably upon annealing, showing the eventual disappearance of columnar structures. Nevertheless, the thickness of the SiOC/Fe interfacial layer remains unaltered, in good agreement with the XRR (see entries for the SiOC + Fe in Table 1). XRR also reveals that in the as-deposited sample, the real part of the SLD of the Fe layer ($54.4*10^{-6}$ Å$^{-2}$) is approximately 14% lower than the SLD of pure Fe ($62*10^{-6}$ Å$^{-2}$). Such a difference may be attributed to light atom impurities, such as H, O, or N, in the Fe layer, giving rise to a lower average density. These impurities may be introduced during deposition.

**Table 1**
Model parameters used to fit XRR data for each sample.

| Layer | Thickness, nm | Re SLD, $10^{-6}$ Å$^{-2}$ | Im SLD, $10^{-6}$ Å$^{-2}$ | Roughness, nm |
|---|---|---|---|---|
| **Untreated** | | | | |
| SiOC | 91.6 | 18 | 0.07 | 3.4 |
| SiOC + Fe | 9 | 43.9 | 0.82 | 5.6 |
| Fe | 78.3 | 54.4 | 1.68 | 3.8 |
| SiO2+Fe | 0.6 | 43.4 | 1.28 | 0.4 |
| SiO2 | 299.7 | 22.5 | 0.1 | 0.3 |
| **200°C** | | | | |
| SiOC | 85.5 | 18.7 | 0.07 | 4.2 |
| SiOC + Fe | 10.3 | 47.4 | 1.30 | 6.3 |
| Fe | 78.5 | 57.2 | 1.65 | 4 |
| SiO2+Fe | 1 | 43.5 | 1.28 | 1.2 |
| SiO2 | 298.8 | 22.5 | 0.1 | 0.5 |
| **400°C** | | | | |
| SiOC | 86.8 | 18.2 | 0.07 | 4.5 |
| SiOC + Fe | 10.5 | 44.3 | 1.51 | 4.7 |
| Fe | 77.5 | 57 | 1.84 | 4.7 |
| SiO2+Fe | 0.7 | 43 | 1.29 | 1.3 |
| SiO2 | 298 | 22.5 | 0.1 | 0.5 |
| **600°C** | | | | |
| SiOC | 85 | 18.5 | 0.08 | 3.6 |
| SiOC + Fe | 13.2 | 41.7 | 1.29 | 5.4 |
| Fe | 53.8 | 62.1 | 3.06 | 2.8 |
| SiO2+Fe | 1.6 | 33.8 | 1.20 | 2.9 |
| SiO2 | 295.9 | 22.5 | 0.1 | 1 |

Upon annealing at 600 °C, the sample undergoes substantial changes. Fig. 4 and Table 1 show that the thickness of Fe layer decreases significantly (from 77.5 nm at 400 °C to about 54 nm, in agreement with the EDS in Fig. 2b) while its SLD increases up to the nominal value for pure Fe. This observation suggests that any light impurity atoms that may have been present in the Fe layer diffused towards the SiOC/Fe interface during annealing and the layer becames fully-dense, pure Fe. These XRR findings are further supported by NR measurements (data not shown), which also revealed the refinement of the Fe layer to its nominal SLD value together with considerable thickness reduction.

Moreover, both EDS and XRR show the thickening of the SiOC/Fe interface up to about 13.2 nm (Fig. 4, insert). Likewise, at 600 °C, the $SiO_2$/Fe interface thickens up to 1.6 nm and its SLD reduces to $33.8*10^{-6}$ Å$^{-2}$ (see Table 1). The SLD of the "$SiO_2$+Fe" layer is consistent with the composition of fayalite ($Fe_2SiO_4$). The composition of the "SiOC + Fe" layer cannot be unambiguously determined based solely on XRR results whose SLD of $41.7*10^{-6}$ Å$^{-2}$ could correspond to either fayalite with inclusions of additional Fe atoms or a simple alloy of Fe:SiOC at 3:2 ratio with a density of ~5.1 g/cc. Since the latter contradicts the Fe:Si ratio at the SiOC/Fe interface obtained by STEM, we conclude that the formation of fayalite layer is the more likely alternative.

### 4.2. RBS

We performed RBS to elucidate the chemical composition of each layer and the degree of intermixing between them. Samples like the one in the present study, which include compositional non-uniformities or mixed compounds, are not easy to characterize by RBS [32]. In addition, RBS is not sensitive to roughness on the free surface. Rather, it senses the multilayer as if the surface were flat and the underlying interfaces rough. Therefore, the main purpose of RBS in the present work is to complement the aforementioned structural analysis by TEM, STEM, EDS, and XRR/NR. Thus, we carry out our RUMP simulation using the probable elemental distribution obtained from XRR.

The RBS data from the bilayer specimen before and after

annealing at different temperatures (200, 400, 600 °C) are shown in Fig. 5 (symbols) together with the RUMP fit (lines). The data in its raw form shows the number of counts as a function of He backscattered energy. The edges of the RBS signal provide a qualitative indication of the Fe (or Si) diffusion distance into the neighboring layer. For example, for the Fe peak, a more gradual slope on the higher energy side indicates intermixing with the SiOC layer while the lower energy side signifies intermixing with $SiO_2$. Fig. 5 shows that neither the Fe peak around 1450 keV nor the Si peak near 1125 keV have sharp, step-like edges, indicating that the interfaces on both sides of the Fe layer are thick, or rough, or both.

The Fe and Si peak shapes in samples annealed at 200 °C and 400 °C are similar to those in the as-deposited sample, indicating that—in agreement with the foregoing sections—the interfacial roughness does not change markedly at these low annealing temperature. The best fit for each RBS data set is obtained with the inclusion of oxygen impurities into the Fe layer consistent with the reduced density of Fe layer deduced from XRR fits (see Table 1). For the sample annealed at 600 °C, the height of Fe peak increases indicating the removal of all impurities from the Fe layer, as observed by XRR. According to XRR, the SiOC/Fe interface thickness after the 400 °C anneal is 10.5 nm and increases by another 2.7 nm upon annealing at 600 °C (Table 1, "SiOC + Fe" layer). The detection of such a small thickness increment of the intermixed layer is beyond the sensitivity of RBS.

### 4.3. Misfit dislocations at Fe/fayalite interface

The presence of misfit dislocations at the Fe/Fayalite interface suggest this interface is incoherent. Previous work has shown that the thickness of this interface fayalite layer does not vary as annealing time goes up, suggesting that this incoherent interface is thermally stable and the Fayalite layer can impede further elemental diffusion [17]. The importance of an incoherent interface has been demonstrated in both metallic nanolaminates and ODS systems which have been shown to be efficient point defect sinks, mitigating radiation damage and helium induced swelling [1,33]. We hypothesize that the Fe/fayalite interface can provide significantly enhanced radiation tolerance, similar to or superior to those observed in metallic nanolayered and ODS structures.

### 4.4. Thermodynamic and DFT modeling

Our experiments suggest that no reaction occurs at either the SiOC/Fe or $SiO_2$/Fe interface at annealing temperatures up to 400 °C. However, after the 600 °C anneal, a 13 nm-thick, thermally stable intermixed layer ($Fe_2SiO_x$) was observed at the SiOC/Fe interface while a thin intermixed layer (as thick as 5 nm, according to EDS, or as thin as 1.6 nm, as determined by XRR) was found at the $SiO_2$/Fe interface. From a thermodynamic point of view, there is a tendency for Fe to react with Si as well as with O to form $Fe_xSi_y$, $Fe_xO_y$, or $Fe_xSi_yO_z$ compounds to lower the overall Gibbs free energy in the SiOC/Fe system. Accordingly, we developed a thermodynamic model to rationalize our experimental results and explain the dependence of interface thickness on temperature.

Among all known Fe, Si, and O ternary phases, the only compound with a Fe:Si ratio of 2 is fayalite: $Fe_2SiO_4$. Fayalite is the most likely product of the reaction of $SiO_2$ and FeO, since other iron oxides with higher iron charge states ($Fe^{3+}$, $Fe^{4+}$) would require $O_2$ as a by-product, which is unlikely under oxidizing conditions. Therefore, we assume the new interlayer phase is indeed $Fe_2SiO_4$ and is formed *via* the following reaction:

$$SiO_2 + 2\,FeO = Fe_2SiO_4. \quad (1)$$

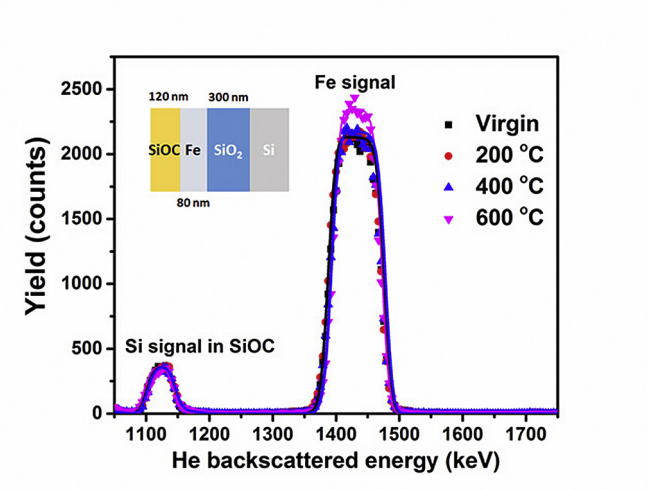


**Fig. 5.** RBS characterization of the bilayer specimen before and after annealing at different temperatures (200, 400, 600 °C). The symbols represent the experimental data and the lines are RUMP fitting results.

Standard thermodynamic data for our model is listed in Table 2 [34,35]. We consider both $SiO_2$ and $Fe_2SiO_4$ phases to have activities of 1. Then, labeling the activity of FeO as $x$, the change of Gibbs free energy at a given temperature (in K) is expressed as:

$$\Delta G_f(T) = \Delta G_f^o + RT\ln\left(1/x^2\right) - T\Delta S_f^o \quad (2)$$

From Table 2, the standard $\Delta G_f^o$ and $\Delta S_f^o$ are both negative, indicating that reaction (1) occurs at standard conditions and becomes progressively less likely as temperature increases.

We solve for the minimum activity of FeO required for the formation of $Fe_2SiO_4$ according to reaction (1) at 600 °C and find that it is 0.439. By contrast, $\Delta G_f^o$ for SiOC is estimated to be 96 kJ/mol lower than that of $SiO_2$ from the typical ~1 eV/$SiO_2$ formula unit enthalpy difference between SiOC and $SiO_2$, determined in one of our previous studies [36]. Therefore, the minimum activity of FeO required for the formation of $Fe_2SiO_4$ from SiOC at 600 °C is 0.0006. Thus, based on our thermodynamics model, at 600 °C, reaction (1) is highly likely at the SiOC/Fe interface, but may be relatively more difficult at the $SiO_2$/Fe interface. This conclusion is consistent with our experiments, which evidence a thick intermixed layer at the SiOC/Fe interface upon annealing at 600 °C while the intermixed layer is at the $SiO_2$/Fe interface is relatively thinner. Our calculation is based on bulk thermodynamic data. However, chemical potentials at surfaces/interfaces are typically higher compared to the bulk [37], further indicating the likelihood of the aforementioned reactions.

Given the negative value of $\Delta S_f^o$ in equation (2), it is surprising that the above mentioned interface reactions occur only after annealing at 600 °C, but not at 400 °C or lower. One possible reason for the 600 °C temperature requirement lies in the fact that FeO only exists as a stable phase above 555 °C according to the Fe–O phase diagram [38]. The relatively limited growth of the $Fe_xSi_yO_z$

**Table 2**
Standard thermodynamic data for the calculations in section 4.

| | $\Delta G^o$ (kJ/mol) | $\Delta H^o$ (kJ/mol) | $S^o$ (J/mol/K) |
|---|---|---|---|
| $SiO_2$ (amorphous) | −850.56 | −903.20 | 47.40 |
| FeO | −251.46 | −271.96 | 60.75 |
| $Fe_2SiO_4$ | −1379.05 | −1479.88 | 145.18 |
| Reaction (1) | −25.57 | −32.76 | −23.72 |

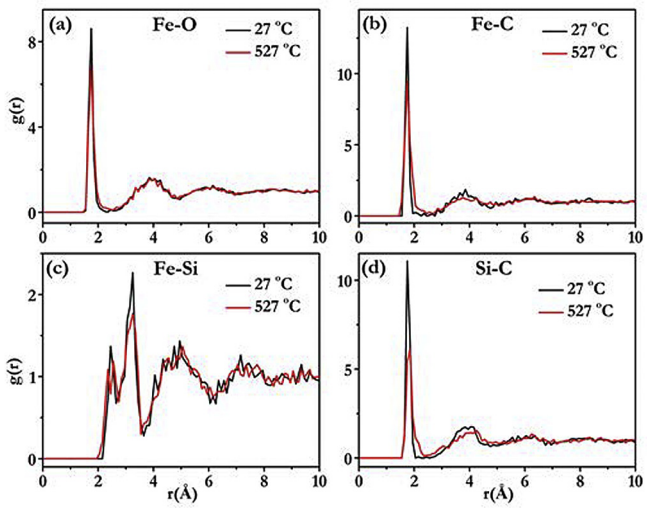


**Fig. 6.** Partial radial distribution functions (PRDFs) after 0.5 ps MD simulations of $Si_{256}Fe_{256}O_{576}C_{192}H_{192}$ at 800 K and 300 K: (a) Fe–O, (b) Fe–C, (c) Fe–Si, and (d) Si–C.

layers subsequent to their formation at 600 °C suggests that, once formed, they may kinetically impede any further reaction between Fe and SiOC or $SiO_2$ [17,39]. This view is consistent with the low diffusivity of Fe, Si, and O in fayalite ($Fe_2SiO_4$) [40].

To gain more insight into the early stages of formation of the intermixed layer, we performed 0.5 ps DFT MD simulations of amorphous $Si_{256}Fe_{256}O_{576}C_{192}H_{192}$ at 300 K and 800 K. This structure is mechanically stable, as evidenced by the limited changes in its partial radial distribution functions, a selection of which is shown in Fig. 6. However, we did observe individual atomic-level rearrangements, which give rise to the changes in the average coordination number of different element types. There is a tendency for the structure to form new Fe–C bonds in place of pre-existing C–H bonds. Fig. 7 illustrates these bond changes, namely the breaking of Si–C and C–H bonds as well as the formation of Fe–C bonds and the evolution of isolated H atoms. The tendency of Fe to react with C leads to an average increase in coordination of Fe by C of ~0.8 Fe–C bond/Fe atom, causing some Fe atoms reach a 6-fold coordination: the same as in $Fe_2SiO_4$. Therefore, our DFT calculations are also consistent with the formation of fayalite at SiOC/Fe interfaces, in agreement with our experimental results.

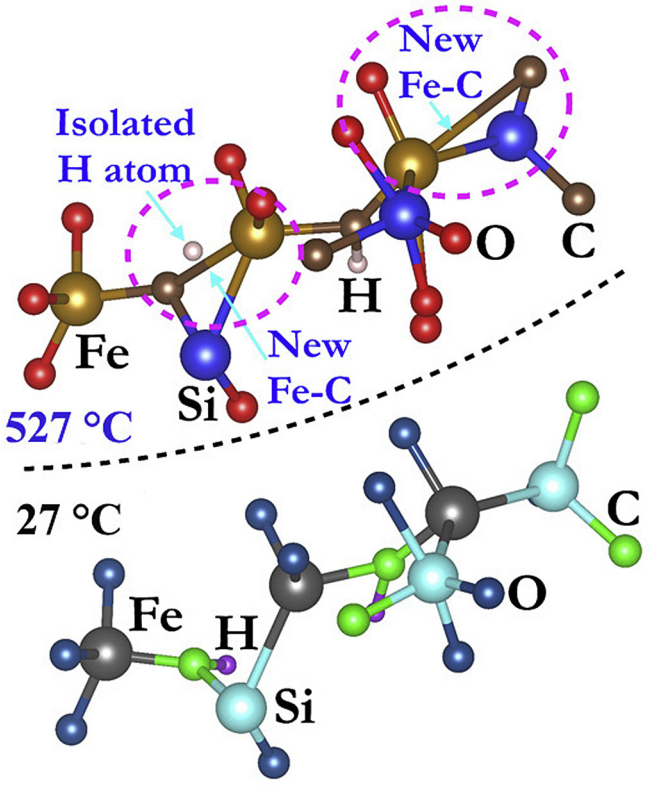


**Fig. 7.** Representative local atomic structure changes in simulated SiFeOCH for structures annealed at 527 °C (800 K) comparing to that at 27 °C (300 K). The atom cluster above the dashed black line is taken from the 800 K model, where large blue is Si, large orange is Fe, red is O, small brown is C, and small purple is H. The atom cluster below the dashed black line is from the 300 K model, where large cyan is Si, grey is Fe, dark blue is O, green is C, and small pink is H. Bonds marked by cyan arrows in pink dashed circles denote newly formed Fe–C bonds. The H atom marked by the cyan arrow in the left pink dashed circle indicates the evolution of an isolated H atom *via* breaking of a C-H bond. (For interpretation of the references to colour in this figure legend, the reader is referred to the web version of this article.)

## 5. Conclusion

The high temperature performance of amorphous-ceramic/metal composites is crucial for their service in extreme irradiation environments. In particular, information about how covalent/metal, amorphous/crystalline interfaces and their impact on radiation response of SiOC/Fe composites is key to the design of composite materials with maximum radiation tolerance. Therefore, we investigated the structure of the interface between amorphous SiOC and crystalline α-Fe in an as-deposited bilayer as well as after annealing at 200, 400, 600 °C for 1 h. The as-deposited interface is thermally stable up to at least 400 °C. Upon annealing at 600 °C, an intermixed layer at the SiOC/Fe interface is observed and it forms incoherent interfaces with Fe and SiOC layers. Both experimental and modeling results suggest that the intermixed layer is crystalline fayalite: $Fe_2SiO_4$. Our work provides a more complete understanding of this new SiOC/Fe interface under high temperature. Future work will focus on the structure of this interface under irradiation, helping the design of radiation tolerant composites for advanced nuclear reactors.

## Acknowledgement

We acknowledge financial support from the DoE Office of Nuclear Energy, Nuclear Energy Enabling Technologies, award DE-NE0000533. The research was performed in part an the Nebraska Nanoscale Facility: National Nanotechnology Coordinated Infrastructure and the Nebraska Center for Materials and Nanoscience, which are supported by the National Science Foundation, Award ECCS: 1542182, and by the Nebraska Research Initiative. Use of the Advanced Photon Source was supported by the US. Department of Energy, Office of Science, under Contract No. DE-AC02-06CH11357. The work at the National Synchrotron Light Source-II, Brookhaven National Laboratory, was supported by the US. Department of Energy, Office of Science, Office of Basic Energy Sciences, under Contract No. DE-SC0012704. This work has benefited from the use of the Asterix reflectometer at the Lujan Center at Los Alamos Neutron Science Center. Los Alamos National Laboratory is operated by Los Alamos National Security LLC under DOE Contract DE-AC52-06NA25396. H. Ding acknowledges computational resources provided by the DOE-National Energy Research Scientific Computing Center under contract No. DE-AC02-05CH11231 and by the Texas A&M High Performance Research Computing program.

## References


[1] G.R. Odette, M.J. Alinger, B.D. Wirth, Recent developments in irradiation-resistant steels, Annu. Rev. Mater. Res. 38 (2008) 471–503.
[2] G.S. Was, Materials degradation in fission reactors: lessons learned of relevance to fusion reactor systems, J. Nucl. Mater 367–370 (Part A) (2007) 11–20.
[3] G.R. Odette, D.T. Hoelzer, Irradiation-tolerant nanostructured ferritic alloys: transforming helium from a liability to an asset, Jom-Us 62 (9) (2010) 84–92.
[4] C.P.C. Wong, R.E. Nygren, C.B. Baxi, P. Fogarty, N. Ghoniem, H. Khater, K. McCarthy, B. Merrill, B. Nelson, E.E. Reis, S. Sharafat, R. Schleicher, D.K. Sze, M. Ulrickson, S. Willms, M. Youssef, S. Zinkle, A. Team, Helium-cooled refractory alloys first wall and blanket evaluation, Fusion Eng. Des. 49–50 (2000) 709–717.
[5] D. Chen, J. Wang, T.Y. Chen, L. Shao, Defect annihilation at grain boundaries in alpha-Fe, Sci. Rep-Uk 3 (2013) 1450.
[6] X.M. Bai, A.F. Voter, R.G. Hoagland, M. Nastasi, B.P. Uberuaga, Efficient annealing of radiation damage near grain boundaries via interstitial emission, Science 327 (5973) (2010) 1631–1634.
[7] A. Misra, M.J. Demkowicz, X. Zhang, R.G. Hoagland, The radiation damage tolerance of ultra-high strength nanolayered composites, Jom-Us 59 (9) (2007) 62–65.
[8] M. Zhernenkov, S. Gill, V. Stanic, E. DiMasi, K. Kisslinger, J.K. Baldwin, A. Misra, M.J. Demkowicz, L. Ecker, Design of radiation resistant metallic multilayers for advanced nuclear systems, Appl. Phys. Lett. 104 (24) (2014).
[9] E.G. Fu, A. Misra, H. Wang, L. Shao, X. Zhang, Interface enabled defects reduction in helium ion irradiated Cu/V nanolayers, J. Nucl. Mater 407 (3) (2010) 178–188.
[10] N. Li, E.G. Fu, H. Wang, J.J. Carter, L. Shao, S.A. Maloy, A. Misra, X. Zhang, He ion irradiation damage in Fe/W nanolayer films, J. Nucl. Mater 389 (2) (2009) 233–238.
[11] R.E. Baumer, M.J. Demkowicz, Radiation response of amorphous metal alloys: subcascades, thermal spikes and super-quenched zones, Acta Mater 83 (2015) 419–430.
[12] J.A. Colón Santana, E.E. Mora, L. Price, R. Balerio, L. Shao, M. Nastasi, Synthesis, thermal stability and the effects of ion irradiation in amorphous Si–O–C alloys, Nucl. Instrum. Methods Phys. Res. Sect. B Beam Interact. Mater. Atoms 350 (2015) 6–13.
[13] M. Nastasi, Q. Su, L. Price, J.A. Colón Santana, T. Chen, R. Balerio, L. Shao, Superior radiation tolerant materials: amorphous silicon oxycarbide, J. Nucl. Mater 461 (2015) 200–205.
[14] Q. Su, B. Cui, M.A. Kirk, M. Nastasi, Cascade effects on the irradiation stability of amorphous SiOC, Philos. Mag. Lett. 96 (2) (2016) 60–66.
[15] Q. Su, L. Price, L. Shao, M. Nastasi, Dose dependence of radiation damage in nano-structured amorphous SiOC/crystalline Fe composite, Mater. Res. Lett. 4 (1) (2016) 48–54.
[16] W.Z. Han, M.J. Demkowicz, N.A. Mara, E.G. Fu, S. Sinha, A.D. Rollett, Y.Q. Wang, J.S. Carpenter, I.J. Beyerlein, A. Misra, Design of radiation tolerant materials via interface engineering, Adv. Mater 25 (48) (2013) 6975–6979.
[17] Q. Su, J. Jian, H. Wang, M. Nastasi, Thermal stability of amorphous SiOC/crystalline Fe composite, Philos. Mag. 95 (34) (2015) 3876–3887.
[18] A.C. Lewis, D. Josell, T.P. Weihs, Stability in thin film multilayers and microlaminates: the role of free energy, structure, and orientation at interfaces and grain boundaries, Scr. Mater. 48 (8) (2003) 1079–1085.
[19] A. Misra, R.G. Hoagland, H. Kung, Thermal stability of self-supported nanolayered Cu/Nb films, Philos. Mag. 84 (10) (2004) 1021–1028.
[20] D. Josell, W.C. Carter, J.E. Bonevich, Stability of multilayer structures: capillary effects, Nanostruct. Mater. 12 (1–4) (1999) 387–390.
[21] S.J. Zinkle, J.T. Busby, Structural materials for fission & fusion energy, Mater Today 12 (11) (2009) 12–19.
[22] Q. Su, L. Price, L. Shao, M. Nastasi, High temperature radiation responses of amorphous SiOC/crystalline Fe nanocomposite, J. Nucl. Mater 479 (2016) 411–417.
[23] Q. Su, B. Cui, M.A. Kirk, M. Nastasi, In-situ observation of radiation damage in nano-structured amorphous SiOC/crystalline Fe composite, Scr. Mater. 113 (2016) 79–83.
[24] L.G. Parratt, Surface studies of solids by total reflection of X-rays, Phys. Rev. 95 (2) (1954) 359–369.
[25] A. Nelson, Co-refinement of multiple-contrast neutron/X-ray reflectivity data using MOTOFIT, J. Appl. Crystallogr. 39 (2006) 273–276.
[26] L.R. Doolittle, Algorithms for the rapid simulation of Rutherford backscattering spectra, Nucl. Instrum. Methods Phys. Res. Sect. B Beam Interact. Mater. Atoms 9 (3) (1985) 344–351.
[27] L.R. Doolittle, A semiautomatic algorithm for Rutherford backscattering analysis, Nucl. Instrum. Meth B 15 (1–6) (1986) 227–231.
[28] G. Kresse, J. Furthmuller, Efficiency of ab-initio total energy calculations for metals and semiconductors using a plane-wave basis set, Comp. Mater Sci. 6 (1) (1996) 15–50.
[29] J.P. Perdew, K. Burke, M. Ernzerhof, Generalized gradient approximation made simple, Phys. Rev. Lett. 77 (18) (1996) 3865–3868.
[30] G. Kresse, D. Joubert, From ultrasoft pseudopotentials to the projector augmented-wave method, Phys. Rev. B 59 (3) (1999) 1758–1775.
[31] M.P. Allen, Molecular graphics and the computer simulation of liquid crystals, Mol. Simulat. 2 (4–6) (1989) 301–306.
[32] Ion Beams for Materials Analysis, Elsevier, 1990.
[33] M.J. Demkowicz, P. Bellon, B.D. Wirth, Atomic-scale design of radiation-tolerant nanocomposites, Mrs Bull. 35 (12) (2010) 992–998.
[34] I. Barin, Thermochemical Data of Pure Substances, Thermochemical Data of Pure Substances, Wiley-VCH, 1997.
[35] I. Gunnarsson, S. Arnorsson, Amorphous silica solubility and the thermodynamic properties of H4SiO4 degrees in the range of 0 degrees to 350 degrees C at P-sat, Geochim. Cosmochim. Ac 64 (13) (2000) 2295–2307.
[36] H.P. Ding, M.J. Demkowicz, Hydrogen reverses the clustering tendency of carbon in amorphous silicon oxycarbide, Sci. Rep-Uk 5 (2015).
[37] P.C. Hiemenz, Principles of Colloid and Surface Chemistry, 1986.
[38] M. Kowalski, P.J. Spencer, Thermodynamic reevaluation of the C-O, Fe-O and Ni-O systems: remodelling of the liquid, BCC and FCC phases, Calphad 19 (3) (1995) 229–243.
[39] L.A. Bendersky, N.V. Kazantseva, U.R. Kattner, K. Wang, V.P. Oleshko, D. Hunter, I. Takeuchi, Interfacial reaction of Co Fe films with SiO2 substrates, Acta Mater 61 (11) (2013) 4180–4190.
[40] D.F. Fisler, S.J. Mackwell, Kinetics of diffusion-controlled growth of fayalite, Phys. Chem. Min. 21 (3) (1994) 156–165.